Influence of Organically Modified Nanoclay on the Performance of Pineapple Leaf Fiber-Reinforced Polypropylene Nanocomposites

Manoranjan Biswal, Smita Mohanty, Sanjay K. Nayak

Laboratory for Advanced Research in Polymeric Materials (LARPM), Central Institute of Plastic Engineering and Technology (CIPET), Bhubaneswar, Orissa 751024, India

Received 2 September 2008; accepted 14 July 2009
DOI 10.1002/app.31121
Published online 19 August 2009 in Wiley InterScience (www.interscience.wiley.com).

ABSTRACT: Polypropylene/Pine apple leaf fiber (PP/PALF)-reinforced nanocomposites were fabricated using melt blending technique in a twin-screw extruder (Haake Rheocord 9000). Variation in mechanical properties, crystallization behavior, water absorption, and thermal stability with the addition of nanoclay in PP/PALF composites were investigated. It was observed that the tensile, flexural, and impact properties of PP increase with the increase in fiber loading from 10 to 30 wt %. Composites prepared using 30 wt % PALF and 5 wt % MA-*g*-PP exhibited optimum mechanical performance with an increase in tensile strength to 31%, flexural strength to 45% when compared with virgin PP. Addition of nanoclay results in a further increase in tensile and flexural strength of PP/PALF composites to 20 and 24.3%, which shows intercalated morphology. However, addition of nanoclay does not show any substantial increase in impact strength when compared with PP/PALF composites. Dynamic mechanical analysis tests revealed an increase in storage modulus (E') and damping factor (tan δ), confirming a strong influence between the fiber/nanoclay and MA-*g*-PP. Differential scanning calorimetry, thermogravimetric analysis thermograms also showed improved thermal properties when compared with the virgin matrix. TEM micrographs also showed few layers of agglomerated clay galleries along with mixed nanomorphology in the nanocomposites. Wide angle X-ray diffraction studies indicated an increase in *d*-spacing from 22.4 Å in Cloisite 20A to 40.1 Å in PP/PALF nanocomposite because of improved intercalated morphology. J Appl Polym Sci 114: 4091–4103, 2009

Key words: nanocomposites; TGA; PALF; TEM; DMA

INTRODUCTION

Recently, natural fiber-reinforced polymer composites have experienced a tremendous growth in the composite industry because of their eco-friendliness and cost effectiveness.[1,2] Compared to inorganic fibers, natural fibers present some advantages, such as low density and price, less abrasive to the processing equipment, harmless, biodegradable, renewable, and their mechanical properties can be comparable to those of inorganic fibers. All these properties have made natural fibers very attractive for industries like the automotive industry that search a product with mechanical properties comparable with glass fiber-reinforced thermoplastics, but lighter and harmless to environment.

Many studies have been developed based on composites containing lignocellulosic fibers from the forest, and paper industry such as cellulose, wood fiber, wood dust; others have been based on agricultural fibers, such as kenaf, sisal, hemp, coir, and rice husk. However, poor hygrothermal resistance and poor adhesion of these fibers towards commercial synthetic resins lead to ineffective interface with the polymer matrix, thereby restricting its extensive use in many structural as well as outdoor applications.[3–5] Thus, surface modification techniques, such as use of coupling agents/compatibilizers, sizing agents, modifiers, plasma treatment, chemical modification through grafting, mercerization, and acetylation, have been commonly used to modify the interface between the natural fibers and the polymer matrix.[6–9] Creations of stress concentration at fiber end and poor interfacial adhesion between the natural fiber and polymer have been recognized as a primary cause of brittleness in these composites. Several research works have been reported on hygrothermal aging of natural fiber, which have been successfully used in various load-bearing applications. Thermoplastic matrices such as polyethylene (PE), polypropylene (PP), polyvinyl alcohol, polystyrene, and polylactic acid have been compounded with natural fibers to fabricate composites with desired attributes.[10–13]

Pine apple leaf fiber (PALF) is a multicellular and lignocellulosic material extracted from the leaves of plant *Ananas cosomus* belonging to the Bromeliaceae family by retting. PALF has a ribbon-like structure

Correspondence to: S. K. Nayak (drsknayak@gmail.com).

and is cemented together by lignin, pentosan-like materials, which contribute to the strength of the fiber. The excellent mechanical properties of PALF associated with high cellulose content and low microfibrillar angle have been taken into consideration for enhancing strength and performance characteristics in the polymer matrix.[6,14] However, relatively few efforts have been taken in studying the reinforcing potential of PALF fibers in developing thermoplastic and thermoset composites using different processing techniques.[7,15]

Clay/polymer nanocomposites have gained a great interest in the past 2 decades since the Toyota group succeeded to prepare a polyamide 6/clay nanocomposite with dramatic property improvements. Increase in mechanical, thermal, and barrier properties, flammability resistance, and heat resistance compared with conventional composites has been the primary reason in the use of these materials for various high performance engineering application, such as aerospace, automotive, construction, infrastructure, and marine.[16–22] Several methods have been adopted to synthesize clay/polymer nanocomposites, wherein the layered silicates can be easily dispersed and the polymer is adsorbed onto the delaminated sheets to facilitate ordered/disordered multilayered intercalated or exfoliated structure. Melt compounding approach has been mostly used to synthesize PP nanocomposites apart from less developed *in situ* polymerization from the nanoclay surface as reported by Vaia et al.[23] Compatibilizers with different molecular weight, percent grafting of maleic anhydride, and in different weight fractions have been used to develop the nanocomposites. Properties of the composites were generally found to be independent of the molecular weight of the compatibilizer andt were strongly dependant on the weight fraction and the extent of grafting of maleic anhydride.[23–25] As most layered silicate platelets are negatively charged, cationic surfactants such as quaternary ammonium ion based are often used to optimize the interaction between the platelets and the polymer.[26]

The effects of organoclays on the mechanical and physical characteristics of a natural fiber polymer composite have not been yet reported. However, there exist some hypotheses that indicate that the introduction of nanoclays in the fiber/polymer system can be satisfactory for enhancing the mechanical properties. The hydrophilic nature of both the natural fibers and the silicates suggests a good compatibility of these two materials to each other. However, to get strong wettability of these two components with the polymer, a compatibilizer agent must be introduced. Commercial copolymer of PP or PE grafted with maleic anhydride (PP-*g*-MA or PE-*g*-MA) can be used for this purpose.

In this investigation, an effort has been made to evaluate the performance characteristics of PP/PALF fiber-reinforced composites filled with organically modified nanoclays. Maleic anhydride-grafted PP (MA-*g*-PP) has been used as the coupling agent to improve the interfacial bonding between the fibers and PP matrix.[27,28] Variation in mechanical properties of PP/PALF composites as a function of nanoclay loading has been evaluated. The composites samples are also subjected to dynamic mechanical analysis measurements to evaluate the glass transition temperature (T_g), stiffness, and damping properties under specific periodic stress. The fractured surface and interfacial adhesion morphology of composites were also observed using scanning electron microscopy (SEM) and transmission electron microscopy (TEM). Thermal stability of samples has been studied using differential scanning calorimetry (DSC) and thermogravimetric analysis (TGA) thermograms. Water absorption and aging behavior were also investigated to evaluate the extent of mechanical degradation in the composites with aging.

EXPERIMENTAL

Materials

Isotactic polypropylene (H110MA) having MFI: 11 g/10 min and density: 0.91 g/cc, obtained from M/s Reliance Industries, Mumbai, India, has been used as the base polymer matrix. Cloisite 20A (C20A), organically treated montmorillonite with dimethyl dihydrogenated tallow quaternary ammonium having cation exchange capacity (CEC) of 95 meq/100 g clay, procured from M/s Southern clay products (Gonzales, TX) and has been used as nanoclay. Epolene® G-3003 having density 0.91 g/cc and acid number 8 with molecular weight of 26,000 was procured from M/s Eastman Chemicals Germany and has been used as compatibilizer. Pineapple leaf fiber (pinus sp.) of 50 μm diameter, procured from SITRA, Coimatore (India), was used as a reinforcing agent. The physical and mechanical properties of PALF fiber are represented in Table I.

Preparation of PP/PALF/clay nanocomposites

The fibers were detergent washed and dried in vacuum oven at 70°C for 24 h before composite preparation. To ensure easy blending of the fibers with the PP matrix, these detergent washed fibers (untreated) were cut into an fiber length of ~ 6 mm using an electronic fiber-cutting machine.

Compounding was carried out using a melt mixer (Haake Rheocord 9000, M/s Haake, Germany) having two banbury rotors and a mixing chamber of 69 cm^3 volumetric capacity. In the first stage, PP/PALF

TABLE I
Physical and Mechanical Properties of PALF

Property	
Density (g/cm^3)	1.44
Diameter (μm)	20–80
tensile strength (MPa)	413–1627
Young's mudulus (MPa)	34.5–82.5
Elongation at break (%)	1.6
Cellulose content	70–80%
Microfibril angle	(0) 8

composites containing different weight percentage of PALF fibers (10, 20, 30, and 40%) with and without MA-*g*-PP at variable weight percent (1, 3, and 5 wt %) were prepared at a temperature of 180°C, with a mixing speed of 40 rpm for a duration of 10 min.

In the second stage, MA-*g*-PP clay master batch was prepared by melt blending MA-*g*-PP with the nanoclay at a screw speed of 50 rpm for 10 min at 200°C. The masterbatch was then subsequently compounded with PP/PALF composites (30% PALF loading). Based on the weight of PP, the clay content was varied from 1 to 3 wt %, and the loading levels of PALF and MA-*g*-PP were fixed at 30 and 5 wt %, respectively, based on the total weight of PP and PALF.

Finally, these premixes were brought to room temperature and compression molded using Delta Malikson Pressman 100T (India) compression molding machine at 190°C temperature to produce sheets of 3 mm ± 0.1 mm thickness.

Mechanical properties

Tensile properties were measured as per ASTM-D 638 with gauge length of 50 mm, at a crosshead speed of 50 mm/min by using Universal Testing Machine (LR 100KLLoyds Instruments, UK).

Flexural properties were measured as per ASTM-D 790 with gauge length of 50 mm, at a crosshead speed of 1.3 mm/min using the same Universal Testing Machine (LR 100KLLoyds Instruments, UK).

Notched izod impact strength of the specimens was evaluated using an Impactometer (Ceast, Italy) as per ASTM-D 256 with a notch depth of 2.54 mm and notch angle of 45°.

Tests for determination of mechanical properties were carried out in a standard temperature of 23°C ± 2°C and 50% ± 2% RH. The data reported are from the average of 10 specimens for each test. Corresponding standard deviations and measurement uncertainty values have also been reported.

Thermal properties

The melting, crystallization, and thermal stability of virgin PP, and the composite and nanocomposite samples have been studied using DSC (Perkin-Elmer Diamond DSC, USA) and TGA (Perkin –Elmer Pyris-7 TGA,), respectively.

DSC analysis was carried out using 5–10 mg of samples at a scanning rate of 20°C/min and at a temperature of 30–200°C under nitrogen atmosphere. Corresponding melting temperature, heat of fusion, and crystallization temperature were recorded.

The thermal stability of the fiber virgin PP and the composites was determined using TGA with samples of ≤5 mg weight and scanned from 40 to 600°C at a heating rate of 20°C under nitrogen atmosphere. The initial and final degradation temperature and corresponding percentage weight loss for the samples were noted.

Morphological analysis

X-ray diffraction

Wide angle X-ray diffraction (XRD) analysis was carried out using Philips X'Pert MPD (Japan), which had a graphite monochromator and a Cu Kα radiation source operated at 40 kV and 30 mA. The basal spacing or *d*-spacing (d_{001}) reflection of the samples was calculated from Bragg's equation by monitoring the diffraction angle, 2θ from 2° to 10°.

Scanning electron microscopy

The SEM of tensile fractured composite specimens was carried out using JEOL-JSM T330A (Germany). The samples were sputtered with platinum and were dried for half an hour at 70°C in vaccum, before study.

Transmission electron microscopy

Samples for TEM imaging were sectioned using Lieca Ultracut UCT microtome. Sections of 50–70 nm thickness were obtained with diamond knife at room temperature. The sections were collected from water on 300 mesh carbon-coated copper grids and were kept overnight on filter paper for drying. Subsequently, TEM of tensile fractured specimens was carried out using JEOL-1200 EX electron microscope at an accelerating voltage of 80 kV.

Optical microscopy

Optical micrographs were obtained by using German Leica DMLP microscope. The samples, sandwiched between two glass plates, were heated to 190°C, held at this temperature for 5 min, and then cooled down naturally to ambient temperature for microscopic observations.

TABLE II
Mechanical Properties of PP/PALF Composites and PP/PALF Nanocomposites

Sample	Tensile strength (Mpa)	SD	Tensile modulus (MPa)	SD	Flexural strength (Mpa)	SD	Flexural modulus (MPa)	SD	Impact strength (J/m)	SD
Virgin PP	17.92	3.03	2143.88	14.14	29.40	4.65	2770	13.04	23.25	5.21
PP/PALF (90/10)	20.14	3.05	2437.18	13.24	31.04	5.72	2814	15.07	22.84	6.34
PP/PALF (80/20)	23.68	4.04	2619.00	15.36	35.94	6.54	2921	13.08	20.06	8.36
PP/PALF (70/30)	25.97	3.26	3812.00	13.23	38.51	3.38	3033	14.12	19.11	5.23
PP/PALF (60/40)	23.62	3.18	3143.78	12.16	37.02	3.61	2817	12.06	18.92	5.18
PP/PALF/MA-*g*-PP (69/30/1)	28.03	2.02	3916.14	11.34	40.12	4.85	3097	16.54	24.28	6.37
PP/PALF/MA-*g*-PP (67/30/3)	30.14	3.63	4201.32	14.31	46.82	4.52	3110	13.03	28.37	5.31
PP/PALF/MA-*g*-PP (65/30/5)	37.62	4.15	4428.59	17.19	52.37	4.54	3217	16.04	31.91	5.17
PP/PALF/MA-*g*-PP/Clay (64/30/5/1)	39.02	4.27	5253.96	18.29	60.28	3.66	3820	12.27	30.12	7.21
PP/PALF/MA-*g*-PP/Clay (63/30/5/2)	42.67	2.63	5723.28	16.24	63.44	3.78	4196	13.46	30.54	7.24
PP/PALF/MA-*g*-PP/Clay (62/30/5/3)	45.14	3.04	6448.12	16.23	65.01	4.84	4458	15.03	29.52	9.29

Fiber content has been fixed to 30 wt % in all MA-*g*-PP composites and clay nanocomposites, whereas PP, MA-*g*-PP, and clay content have been varied.
SD, standard deviation.

Fourier transformation infrared spectroscopy

FTIR spectra of virgin PP and PP/PALF/C20A composites grafted with maleic anhydride were recorded using Perkin-Elmer 1720X (U.K) spectrometer. Each spectrum was obtained by adding 64 consecutive scans with a resolution of 4 cm^{-1} within the range of 500–4000 cm^{-1}. The samples were studied using two different methods. The FTIR analysis of virgin PP and PP/PALF/MA-G-PP with C20A was studied using cast film method. A uniform and continuous film was formed on the disk till the solvent evaporated completely.

Water absorption test

Water absorption test of PP/PALF and PP/PALF/C20A composites was performed as per ASTM-D 570. Specimens were dried at 80°C in a vacuum oven until a constant weight was attained. Subsequently, they were immersed in water in a thermostated stainless steel water bath at 30°C. Weight gain was recorded by periodic removal of the specimens from the water bath and weighing on a balance with a precision of 1 mg. The percentage gain at any time as a result of moisture absorption was determined.

Dynamic mechanical properties

The dynamic mechanical behavior of the samples was studied using dynamic mechanical thermal analyzer (NETZSCH DMA 242). The experiments are carried out at fixed frequency of 1 Hz and at a heating rate of 10°C/min. The tests were conducted in a temperature range of −150 to 200°C using specimen of dimensions 40 mm × 10 mm × 3 mm.

RESULTS AND DISCUSSION

Mechanical properties

Effect of fiber loading on mechanical properties of PP/PALF composites

The mechanical properties of PP/PALF composites at variable weight percentage of PALF fibers are represented in Table II. It is evident that with an increase in the PALF fiber content from 10 to 30% there is a linear increase in the mechanical properties of the composites. Nearly, 31% increase in the tensile strength and 45% increase in flexural strength were observed with the incorporation of 30 wt % of PALF fiber. A similar increase in tensile and flexural modulus was also observed. However, incorporation of PALF fibers resulted in decrease in the impact strength of the PP matrix from 23.25 to 19.11 J/m, respectively, at 30% loading of PALF, which may be due to nonuniform dispersion of fiber in the matrix. The composites prepared using PALF fiber loading of 40 wt % exhibited deterioration in mechanical properties, which is probably due to improper wetting of the fibers within the matrix that results in microcrack formation at the interface as well as nonuniform stress transfer due to fiber agglomeration within the matrix. Similar investigation have also been reported by Mohanty et al.[30] for jute-reinforced polyester amide composites in which the broken fiber ends caused crack initiation and potential composite failure at 53% fiber loading. Rana et al.[31] have also investigated a decrease in the impact strength by 17% in jute PP composites as the fiber loading was increased from 30 to 60 wt %. Similar facts have also been substantiated in our experimental results. Composites prepared at 30 wt % of fiber loading

have been taken for compatibilization with MA-*g*-PP.

The hydroxyl and the polar groups located in the branched heteropolysaccharides present in the PALF fibers are active sites of water absorption that result in incompatibility with hydrophobic PP matrix and leads to weak interface and hence poor mechanical properties. Addition of MA-*g*-PP resulted in significant increase in the mechanical properties of PP/PALF composites, which is in agreement with the results established in the literature.[6,14] MA-*g*-PP acts as a dispersing agent between the nonpolar fibers and the polar matrix resulting in improved interfacial adhesion, which contributes to enhanced stress transfer from the matrix to the fiber via the compatibilizer. The composites prepared at 30% PALF loading and 5 wt % of MA-*g*-PP exhibited optimum mechanical strength. It was observed that the tensile strength increased to 44% with flexural and impact strength to 36 and 67%, respectively, when compared with PP/PALF composites without MA-*g*-PP. This behavior primarily attributed to the fact that the anhydride group of MA-*g*-PP reacts with the hydroxyl group of PALF fibers forming an ester linkage at the interface. Furthermore, the high-molecular-weight MA-*g*-PP has more flexible PP chains, which are able to diffuse into the matrix leading to interchain entanglements, thereby contributing to the mechanical continuity of the system. However, increase in the MA-*g*-PP content to 7 wt % resulted in decrease in the mechanical strength of the composites, and the data for the same have not been reported in this context. This is probably due to self-entanglement among the compatibilizer chains rather than with the polymer matrix resulting in slippage.

Effect of nanoclay on the mechanical properties of PP/PALF composites

As the composite samples at 30% fiber loading and 5% MA-g-PP show optimum properties, this composition has been taken for fabrication of nanocomposites and for further characterization studies. The mechanical properties of PP/PALF composites at 30% PALF loading with and without MA-*g*-PP and containing different weight percentage of nanoclay loading are depicted in Table II. As observed from Table II, with incorporation of nanoclay from 1to 3 wt% the tensile and flexural strength of PP/PALF composites increases. The tensile and flexural strength increased to 20 and 24.3% between 1 and 3 wt % of clay loading. Similarly, the tensile and flexural modulus showed a linear increase with the increase in the clay content. However, addition of nanoclay decreased the impact strength of MA-*g*-PP-treated PP/PALF composites to about 7.5%. Further increase in clay loading from 5 to 7 wt % did not show any appreciable increase in the mechanical properties of the composites.

Test results indicated that addition of nanoclay improves the mechanical properties of PP/PALF composites. Presence of 5 wt % of MA-*g*-PP might have also contributed in improvement in mechanical properties. This indicates that the multistage process used in the fabrication of nanocomposites, i.e., melt blending of MA-*g*-PP with nanoclay followed by addition of PP/PALF composites resulted in exfoliation of clay galleries. The exfoliated PP/PALF/C20A nanocomposites thus shows better performance over the PP/PALF composites, suggesting improved fiber/nanoclay matrix interfacial adhesion. The mechanical findings are in agreement with the morphological interpretations from wide angle XRD and SEM discussed in the later sections. However, the impact strength in the nanocomposites did not show any appreciable change with the incorporation of nanoclays. Similar results have also been reported by Lei et al.,[32] wherein a decrease in the impact strength of HDPE/pine/clay nanocomposites was observed. Possibility of counteraction between two different fillers, i.e., nanoclay and the fibers, might have caused negative impact performance of the system. Further, investigation in the use of high molecular weight/higher acid number, maleic anhydride-grafted PP could enhance the nanocomposite performance.

Thermal properties

Differential scanning calorimetry

Figure 1 shows the heating and cooling curves of DSC analysis of virgin PP, PP/30%PALF/5%MA-*g*-PP composites along with PP/30%PALF/5%MA-*g*-PP/3%C20A nanocomposites. Melting point and crystallinity of all the samples were investigated using DSC and are shown in the Table III. The melting temperature (T_m) of the virgin polymer and PP/PALF composites at 30% PALF loading and nanocomposites was taken as the maximum of the endothermic peak obtained from the second heating, whereas the crystallization temperature (T_c) was taken as the maximum of the exothermic peak from the cooling cycle. It was observed that the T_m of the virgin matrix decreased with the incorporation of fibers and nanoclays. Comparing the DSC cooling thermograms of pure PP with respect to PP/PALF composites, it is observed that the T_c of virgin PP was about 104.43°C, with a degree of crystallinity X_c of 51.1% (Table III). Incorporation of 5 wt % MA-*g*-PP in PP/PALF composite matrix results in an increase in T_c to 110.74°C, which may be attributed to the presence of PALF fibers that restricts the chain

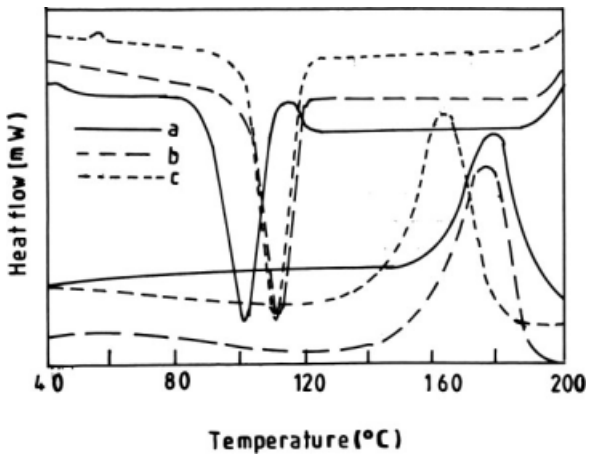

Figure 1 DSC heating and cooling curve of (a) PP (V), (b) PP/PALF/MA-*g*-PP, and (c) PP/PALF/MA-*g*-PP/C20A.

mobility of the matrix chains. However, the degree of crystallinity X_c decreased to 40.6% suggesting that presence of MA-*g*-PP reduced the perfection of PP crystals. Nevertheless, addition of MA-*g*-PP to PP/PALF/C20A system increased the crystallization rate suggesting that exfoliated clay and PALF with aid of MA-*g*-PP acts as nucleating agent and lowers PP crystal perfection. The same has been confirmed using optical microscopy displayed in Figure 2. It is evident from Figure 2(a–c) that incorporation of fibers and nanoclays may act as nucleation agents in the PP matrix during crystallization of PP/PALF composites and nanocomposites owing to strong interaction between nanoclays, fiber, and matrix polymer. The heterogeneous nucleation effect of the fibers, wherein number of nucleus generated from the nucleation agent, simultaneously grow in a limited space and lead to the formation of small-size crystals. In addition, these nuclei centers will also cause more crystalline defects and confine the movements of polymer chains that results in producing stress in crystals. Further, the spherulite size decreases dramatically with the incorporation of C20A, wherein typical spherulites could not be observed. It is also evident that the dispersed fibers and silicate layers provide the substrates of PP nucleation. This further contributes to a decrease in crystallinity in these composites and nanocomposites.

The DSC melting temperature of the matrix polymer in PP/PALF composites, however, decreased because of the lower melt viscosity when compared with virgin PP. The lower melting point and temperature of crystallinity as well as the differences in

TABLE III
Melting and Crystallization Behaviour of Virgin PP, MA-*g*-PP Compatibilized PP/PALF Composites, and PP/PALF/C20A Nanocomposites

Sample	T_m (°C)	T_c (°C)	ΔH (J/g)	X_c (%)
Virgin PP	178.68	104.43	122.9	51.10
PP/PALF/MA-*g*-PP	175.62	110.74	97.65	40.60
PP/PALF/MA-*g*-PP/C20A	166.60	110.67	108.65	45.17

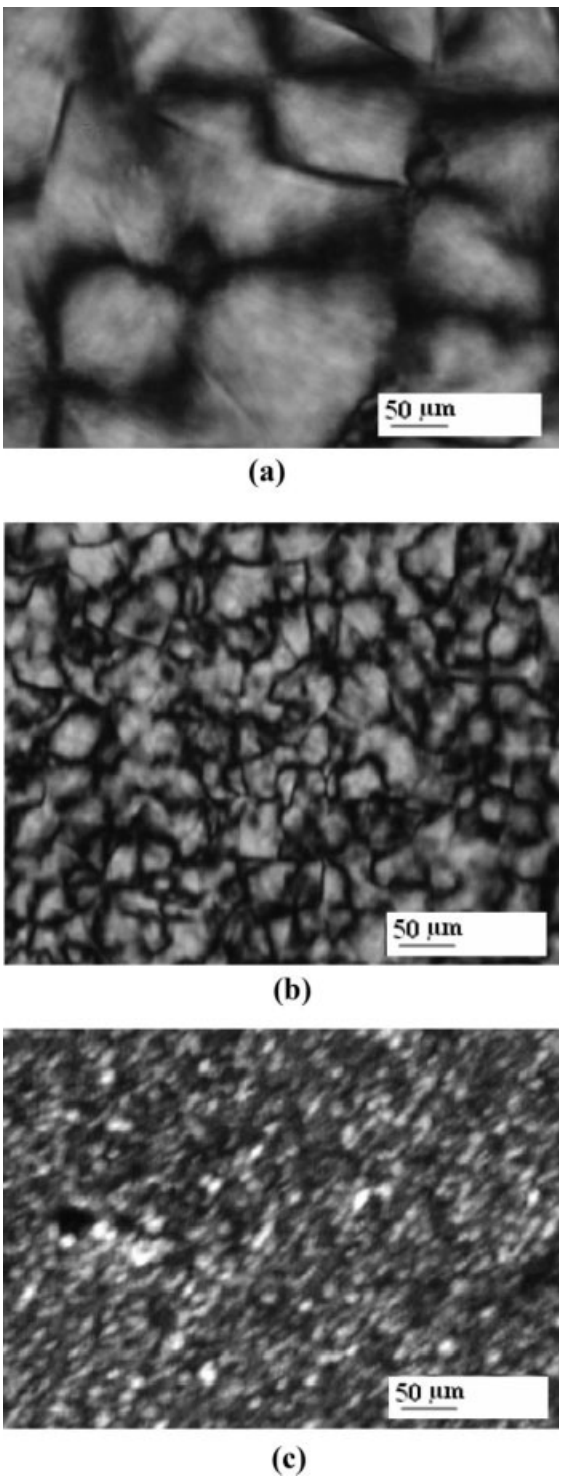

Figure 2 Optical microscopy of (a) PP (V), (b) PP/PALF/MA-*g*-PP, and (c) PP/PALF/MA-*g*-PP/C20A.

TABLE IV
TGA Thermograms of Virgin PP, MA-*g*-PP Compatibilized PP/PALF Composites, and PP/PALF/C20A Nanocomposites

Sample ID	Initial decomposition temperature (°C)	Final decomposition temperature (°C)	Temperature at 50% weight loss (°C)	Charred residue (%)
PP	246	426	371.7	2.4
PP/PALF/ MA-*g*-PP	249	432	374.2	4.2
PP/PALF/ MA-*g*-PP/20A	252.6	451	400.1	7.8

degree of crystallinity indicate that the crystallization process is affected, and thatt the crystals formed are smaller. Crystals start growing from the fibers in the perpendicular direction, an effect known as transcrystallization. This perpendicular growth continues until it is interrupted by the presence of another fiber. Thus, on one hand the fibers act as nucleation sites for the crystal growth, whereas on the other side they can also interrupt it. Further, incorporation of nanoclay additionally reduced the melting point of the composite matrix while increasing its crystallinity level, which clearly indicates that the nanoclay acts as a nucleating agent promoting nucleation sites.

The degree of crystallinity has been estimated using the following equation

$$X_c\ (\%) = \frac{\Delta H_f}{\Delta H_{100\%}} \times \frac{100}{(1 - \mathrm{Ww})},$$

where X_c is the percentage of crystallinity, ΔH_f is the experimental melting heat of fusion, $\Delta H_{100\%}$ is the heat of fusion of 100% crystalline PP, and Ww is the weight fraction of nanoclay.

Thermogravimetric analysis

The TGA thermograms of virgin PP, PP/PALF composites, PP/PALF/C20A nanocomposite with MA-*g*-PP are represented in Table IV. It is evident that the thermal degradation of virgin PP started at 246.2°C and 100% degradation was noticed at 426°C. In the case of PALF fiber, dehydration and degradation of lignin occurred around 40–275°C and maximum percentage of cellulose was found to decompose at a temperature of 380°C from literature. The initial moisture absorption in case of PALF fibers was not noticed in this case, which is probably due to detergent treatment of the fibers that results in rough surface topology as well as removal of lignin. This decomposition temperature range was comparatively less than that of virgin PP. PP/PALF composites with MA-*g*-PP exhibited an initial decomposition peak between 249 and 342.3°C with a maximum of 312.6°C corresponding to a weight loss of about 20%. This was probably due to dehydration from cellulose unit and thermal cleavage of glycosidic linkage by transglycosylation and scission of C—O and C—C bonds. The second decomposition occurred around 361 and 432°C. The weight loss at this temperature was about 86%, which primarily attributed to aromatization, involving dehydration reaction. At 426°C, PP got completely decomposed, wherease in the composites a charred residue of carbonaceous product of 2.1% was left. However, with the incorporation of nanoclays, there was substantial enhancement in the thermal stability of PP/PALF composites with an initial degradation decomposition peak at 252.6°C and final decomposition peak at 451°C. The increase in thermal stability of nanocomposites is attributed to the organic/inorganic interaction between the polymer and nanoclays. By comparing the thermal stability and weight loss with the PP/PALF composites, it is observed that the weight loss at final decomposition temperature is higher for the nanocomposite samples. The enhanced thermal stability is attributed to strong interaction of base polymer and clay surface through chemical linkage between compatibilizer and nanoclays, which in turn mediates the surface polarity of the clay and the polymer/clay interface. The organoclay delays volatilizations of the products generated at the temperature of carbon—carbon bond scission of the polymer matrix.[32–37] Moreover, the nanocomposites samples displayed higher charred residues, indicating over PP virgin showed improve flame resistance.

Morphological analysis

Wide angle X-ray diffraction

The changes in the interlayer distance of clay can generally be elucidated using XRD. A shift to lower angles in the peak represents the formation of an intercalated structure, whereas the disappearance of the peak signals leads to the potential existence of an exfoliated structure. The d_{001} spacing was calculated from peak positions using Bragg's Law, $2d \sin\theta = n\lambda$ where, λ is the X-ray wave length (1.54 Å). Figure 3 and Table V display the wide angle XRD patterns of C20A, PP/C20A, and PP/PALF/20A nanocomposites.

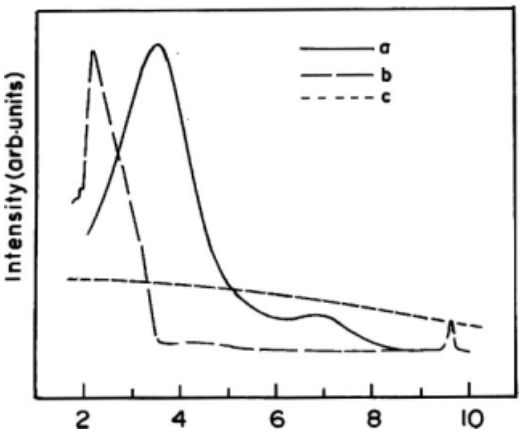

Figure 3 Wide angle X-ray diffraction pattern of (a) Cloisite 20A, (b) PP/PALF/C20A, and (c) PP/PALF/MA-*g*-PP/C20A.

The XRD pattern of modified clay C20A reveals a reflection peak at $2\theta = 4^\circ$ with a *d*-spacing of 24.2 Å. PP/C20A nanocomposites displayed a shift of diffraction peak to $2\theta = 3.15^\circ$, with *d*-spacing of 28 Å thus indication of intercalated structure. Further, the incorporation of nanoclay to PP/PALF composites resulted in further shifting of the diffraction peak to lower angles at $2\theta = 2.2^\circ$ with *d*-spacing of 40.1 Å. This increase in interlayer distance of C20A with the incorporation of PALF is probably due to strong shearing forces that resulted during processing of PP/PALF/C20A nanocomposites.[19,38–42]

Further, the XRD patterns of MA-*g*-PP compatibilized PP/PALF/C20A nanocomposites revealed absence of diffraction peak within the experimental range, thus indicating exfoliation of the clay galleries. This behavior is probably due to the fact that MA-*g*-PP molecules act as a compatibilizer and could enter and penetrate into the clay galleries because of stronger hydrogen bonding between maleic anhydride group of MA-*g*-PP and oxygen groups of C20A at the interface. This strong bonding contributes to an increase in gallery spacing of clay thereby allowing the PP chains to enter and break the clay galleries during compounding, hence resulting in an exfoliated and well-dispersed clay structure. Similar results have also been reported by Lei et al.,[32] where in the interlayer spacing of clay layers increased with the incorporation of pine flour in HDPE wood composites.

TABLE V
Wide Angle XRD Results with Clay Content

Sample	Diffraction peak (0)	*d*-spacing (Å)
Cloisite 20A	4	24.2
PP/C20A	3.15	28
PP/PALF/C20A	2.2	40.1

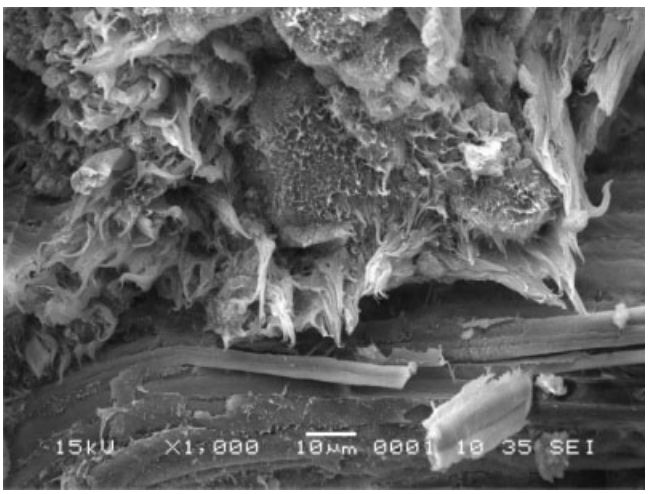

Figure 4 SEM micrographs of PP/PALF composites without MA-*g*-PP.

Scanning electron microscopy

The morphology of the tensile fractured surfaces of PP/PALF composites with and without MA-*g*-PP is depicted in Figures 4 and 5, respectively. Figure 4 reveals extensive fiber pullouts and wide gaps between the fiber and PP matrix in case of PP/PALF composites without MA-*g*-PP, whereas in presence of MA-*g*-PP compatibilizer the fibers were well coated and embedded within the PP matrix as shown in Figure 5. This indicates poor interfacial adhesion and inadequate wetting of the untreated fibers within the PP matrix in case of the composite samples without MA-*g*-PP, which is probably due to a large difference in the surface energies between the fibers and the matrix. However, in the presence of MA-*g*-PP, the fibers are pulled out together with the PP matrix during fracture in tensile test, which further substantiates cohesive coupling between

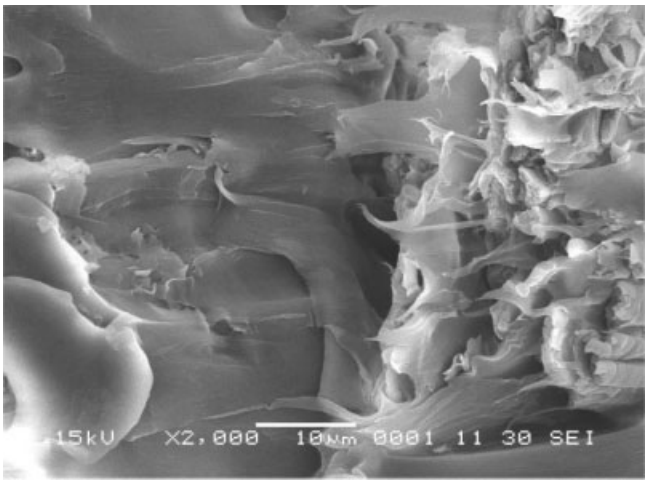

Figure 5 SEM micrographs of PP/PALF/20A nanocomposites with MA-*g*-PP.

MA-*g*-PP, fibers and PP matrix revealing efficient fiber matrix adhesion. Figure 5 also reveals that the compatibilizer is adhered to the primary cell wall of the fiber and the crack has not run through the fiber matrix interface or perpendicular to the fiber but it has fully split over the fiber length. Evidence of pull out is also observed, which may be a small part of the secondary cell wall, i.e, adhered to the PP matrix. In the case of PP/PALF/C20A nanocomposites samples, addition of nanoclay to PP/PALF composites in presence of MA-*g*-PP exhibited improved dispersion of PALF fibers within the PP matrix with considerable reduction in the gaps between the fiber and the matrix. However, SEM micrographs of the PP/PALF composites and PP/PALF/C20A nanocomposites with MA-*g*-PP could hardly show any phenomenal morphological distinction. Hence, TEM micrographs of the nanocomposites samples could possibly substantiate the dispersion of the clays within the PP/PALF composites system.

Transmission electron micrographs

The arrangement of clays within the PP/PALF/MA-*g*-PP/C20A nanocomposite is observed by transmission electron micrographs. Figure 6 reveals that intercalated clay galleries as well as stacks of agglomerated clays galleries were noticed within the PP/PALF/C20A nanocomposites. The dark lines represent the thickness of individual clay layers or agglomerates. Thick darker lines represent stacked silicate layers due to clustering or agglomeration. It can also be observed from the figures that a much brighter zone probably corresponding to a void left in the place where a fiber was placed. The presence of clay agglomerates around the perimeter of the void implies the possible interaction of the clays with the fiber previously placed in that void. This implies that the adhesion between the fiber and the matrix is not good, and during the preparation of samples for TEM by microtomy, fibers fall off leaving voids. Regions of intercalated clay galleries along with intercalated stacks were also evidenced in the TEM micrographs of PP/PALF/MA-*g*-PP/C20A nanocomposites, which further confirmed improved interface due to formation of chemical/physical bonds.

Fourier transformation infrared spectroscopy analysis

The formation of interfacial bonds in the system was further studied using Fourier transformation infrared spectroscopy. IR spectroscopy can be used to examine the manner in which the polymer is arranged and associated within clay-layered structure. FTIR spectra of virgin HDPE and MAPE copolymer are depicted in Figure 7(a). It is evident that the backbone molecule polyolefin presents a strong

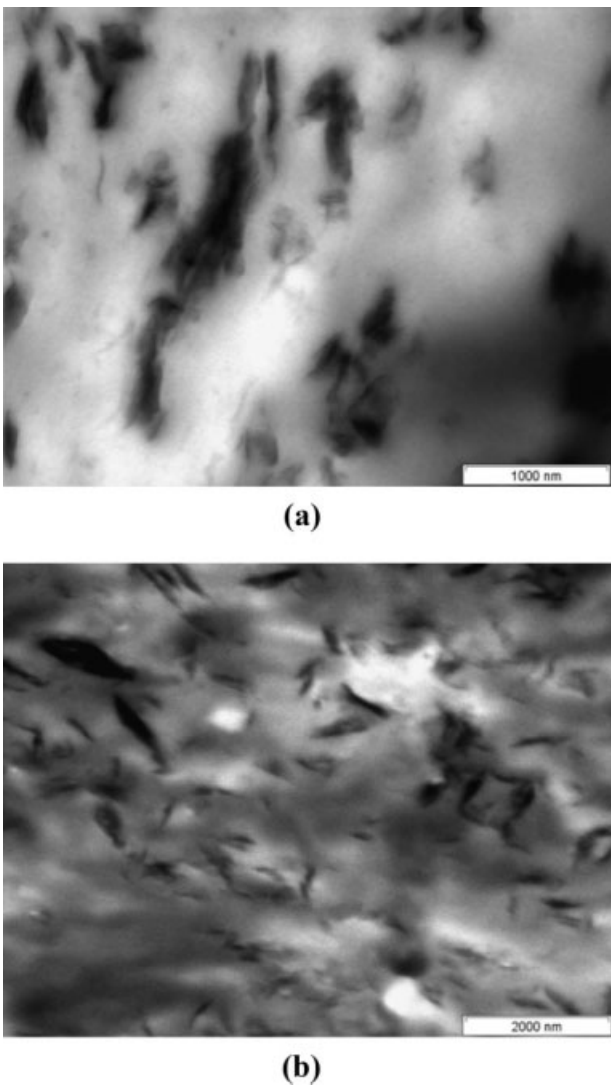

Figure 6 Transmission electron micrographs of PP/PALF/MA-*g*-PP/C20A nanocomposites at (a) 1000 nm and (b) 2000 nm magnifications.

peak of (—C—H) corresponding to 2923 and 1466 cm^{-1} with a moderate peak of ($—CH_2—$) around 720 cm^{-1}. Methyl groups ($C—CH_3$) also presented a significant peak at 2850 cm^{-1}. MAPP copolymer exhibited characteristic peaks between 1800 and 1700 cm^{-1} [Fig. 7(b)], respectively. Bands corresponding to cyclic anhydrides were also observed within the range of 1800 and 1700 cm^{-1}, separated by about 60 cm^{-1}. The peak at low frequency of 1717 cm^{-1} was more intense than at high frequency of 1790 cm^{-1}. Figure 7(c) depicts the FTIR spectra of untreated and MAPP-treated composites, respectively. As observed from the figure, the untreated composites exhibited a peak around 3400 cm^{-1}, which was mainly due to absorption of water by PALF fiber. Similar phenomenon was also observed in the case of the MAPP-treated composites. However, the treated composites displayed a strong band

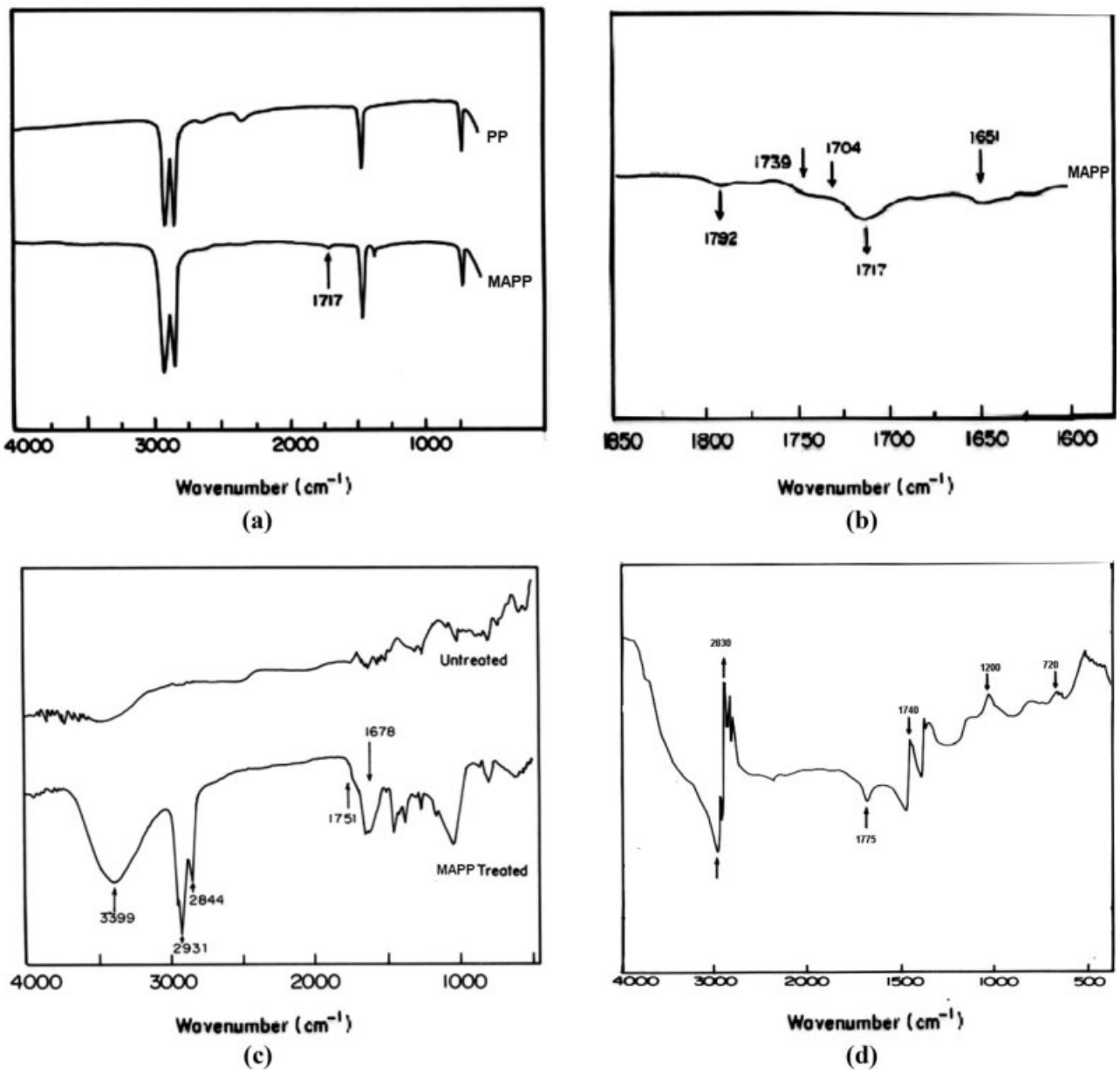

Figure 7 FTIR spectra of (a) virgin PP, (b) MAPP copolymer, (c) untreated and MAPP-treated composites, (d) MA-*g*-PP copolymer PP/PALF/MA-*g*-PP/C20A nanocomposites.

corresponding to 2931 and 2844 cm^{-1}, respectively, indicating the characteristic spectra of PE. Furthermore, a peak observed around 1751 cm^{-1} in these composites confirms the presence of ester linkage at the interface. The formation of ester linkage at the interface has also been reported by Mohanty et al.[30] and Botev et al.[29] for jute and basalt fiber-reinforced PP composites, respectively. The featured peak of cyclic anhydrides appeared at 1717 cm^{-1}, thus suggesting the existence of free or ungrafted maleic anhydride groups at the interface that is probably due to limitation on graft polymerization.[41]

Conversely, in case of PP/PALF/MA-*g*-PP-C20A nanocomposites [Fig. 7(d)], the stretching peak of keto group (—C=O) in the region around 1775 to 1740 cm^{-1} indicates the anhydride group and H-bonding between the fibers and matrix. The bending peak corresponding to 720–1000 cm^{-1} represents tertiary alkyl groups, which is absent in all the other samples. Also, the peak of fatty acids in C20A of (—C=O) group in the region of 1000–1200 cm^{-1} ,which is absent in other cases, confirms the interaction between the clay, fibers, and matrix.

Water absorption test

The influence of PALF fiber and clay on the moisture stability of PP/PALF composites and PP/

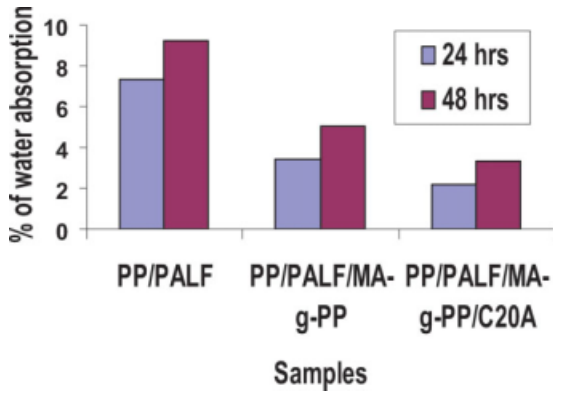

Figure 8 Water absorption characteristics of Column 1. PP/PALF, Column 2. PP/PALF/MA-*g*-PP, Column 3. PP/PALF/MA-*g*-PP. [Color figure can be viewed in the online issue, which is available at www.interscience.wiley.com.]

PALF/C20A nanocomposites is shown in Figure 8. It is evident from the test results that there is a linear increase in the water absorption in all the samples. PP/PALF composite sample exhibited a greater tendency of water absorption, which is due to hydrophilic nature of PALF fibers. However, in the case of PP/PALF/C20A nanocomposites, the exfoliated clay galleries created longer diffusion paths, thereby resulting in less water absorption.

Dynamic mechanical analysis

Storage modulus (E')

The elastic component, E', is a measure of load-bearing capacity of a material and is analogous to flexural modulus E, determined in accordance with ASTM-D 790. The variation of storage modulus as a function of temperature for different samples is graphically represented in Figure 9. It is evident that by addition of PALF fibers the modulus of the virgin matrix increased. This behavior is primarily attributed to the reinforcing effect imparted by the fibers that allowed a greater degree of stress transfer at the interface.

A comparative higher magnitude of E' was observed with the PP/PALF fiber-reinforced nanocomposites over the entire range of temperature, thus showing improved dispersion of the nanoclays within the matrix. In all the samples, the storage modulus decreased with the increase in temperature and exhibits a significant fall between −20 and 10°C, which probably due to glass transition region of the matrix. In case of virgin PP, the storage modulus drops steeply on increasing the temperature because of increased segmental mobility of the polymer chains. However, incorporation of PP/PALF fibers and nanoclay reduces the rate of fall of the matrix modulus with temperature, thus indicating higher

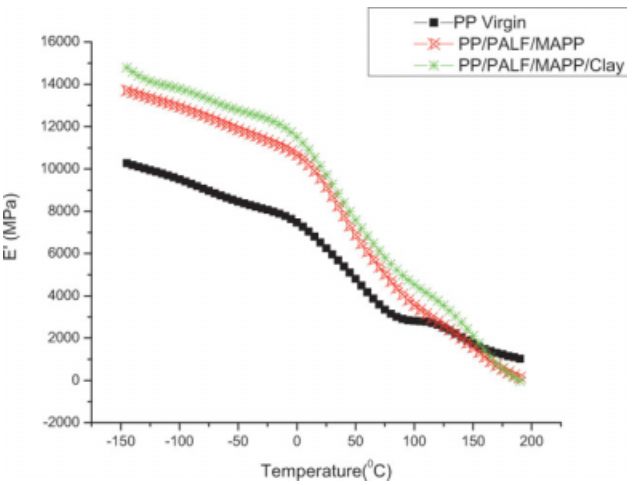

Figure 9 Storage modulus of PP nanocomposites with respect to virgin PP. [Color figure can be viewed in the online issue, which is available at www.interscience.wiley.com.]

stability of PP in the fiber-reinforced nanocomposite system.

Loss modulus (E'')

PP shows three relaxation peaks at −114°C (γ), 13.6°C (β), and 116.9°C (α), respectively. The temperature of β relaxation maximum corresponds to the T_g of the matrix, whereas α relaxation peak is related to the slip mechanism in the crystallites. The γ relaxation peak is due to the motion of small chain groups such as methyl and methylene. In this study, α and β relaxation phenomenon of virgin PP, PP/PALF, and PP/PALF/C20A nanocomposites with MA-*g*-PP has been investigated from loss modulus (E'' curves) represented in the Figure 10. In the case of virgin PP, the maxima of the peak at a temperature of 10.6°C are associated with the T_g of the

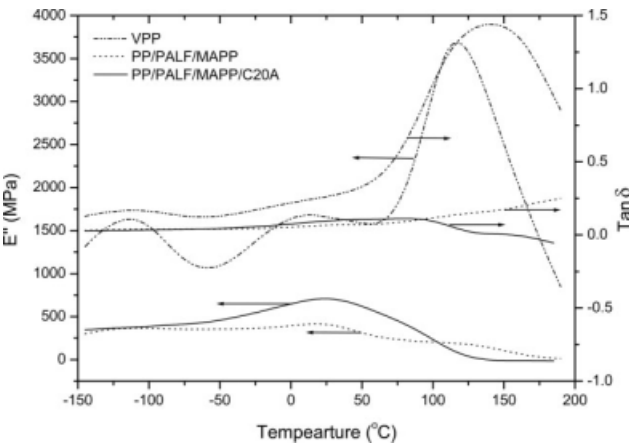

Figure 10 Loss modulus and loss tangent of PP nanocomposites with respect to virgin PP.

matrix, whereas the high temperature peak at 116.9°C is probably related to the onset of melting of PP crystallites. In the case of PP/PALF composites, the primary transition peak, that is T_g, is shifted to higher temperature. This is primarily attributed to immobilization of polymer molecules near the surface of PALF fibers due to molecular interaction caused by the latter.

Further, with the addition of nanoclay, a marginal decrease in the T_g of PP/PALF composites was observed, which indicates the presence of a genuine interface. In the case of the filled systems, broadening of the relaxation region was observed that is probably due to inhibition of relaxation process resulting in decrease in the chain mobility in the crystallites.

Loss tangent (tan δ)

The variation of the tan δ is a function of temperature and is illustrated in Figure 10. The damping peak in the PP/PALF and PP/PALF/C20A nanocomposites showed a decreased magnitude of tan δ and broadening of the PP transition region in comparison to virgin PP. This is mainly due to the fact that the fibers carry a greater extent of stress and allow only a small part of it to strain the interface. Therefore, energy dissipation will occur in the polymer matrix and at the interface, with a stronger interface characterized by less energy dissipation. This fact is substantiated in our experimental results that further revealed efficient fiber matrix adhesion with the addition of MA-*g*-PP. The PP/PALF composites, however, exhibit a high magnitude of tan δ above the glass transition region when compared with PP/PALF/C20A nanocomposite system indicating lesser, interfacial fiber/matrix bond and fibrillation of fibers.

CONCLUSIONS

The mechanical, thermal, dynamic mechanical, and morphological properties of the PP/PALF nanocomposites have been investigated.

- PP/PALF nanocomposites were prepared using melt compounding technique.
- Composites prepared at 30 wt % of fiber loading with 5% MA-*g*-PP showed optimum mechanical performance.
- Incorporation of 3 wt % of cloisite 20A additionally increases the mechanical and thermal properties of PP matrix.
- Morphological observations confirmed efficient dispersion of nanoclays and intercalation of the polymer segments in the gallery space in case of organically modified nanocomposites.
- DSC measurements revealed that the fiber-reinforced nanocomposite system displayed less T_m, which reveals presence of a genuine interface. However, T_c of the virgin matrix increase in the composites and nanocomposites, which shows that incorporation of fibers and nanoclays may act as nucleation agents in the PP matrix during crystallization of PP/PALF composites and nanocomposites owing to strong interaction between nanoclays, fiber, and matrix polymer.
- The storage modulus increased with the incorporation of the nanoclays. The tan δ of the blend matrix displayed two distinct transitions corresponding to α, β of PP matrix.
- The T_g of the matrix shifted to high temperature regions with the incorporation of clays and fibers.
- TGA thermograms also revealed a higher thermal stability of the blend matrix in presence of nanoclays.
- For PP/PALF nanocomposites, a good balance of properties in terms of stiffness and strength can be achieved at an optimal concentration of fibers, clays, and MAPP.

References

1. Yong, L.; Qinglin, W.; Craig, M.; Clemons, Fei, Y.; Yanjun, X. J Reinf Plast Compos 2007, 22, 3959.
2. Thwe, M. M.; Liao, K. Composite 2002, 33, 43.
3. Plackett, D. Presented at the 7th Toronto Conference on "Progress in Woodfibre-plastic Composites", Toronto, Canada, 2002.
4. Ellison, G. C.; McNaught, R. (2000). Research and development report of ministry of agriculture fisheries and food agri – industrial materials, Reference NF0309, 10 Whitehall Place London SW1A 2HH, February 2000.
5. Felix, J. M.; Gatenholm, P. J Appl Polym Sci 2001, 42, 609.
6. George, J.; Bhagawan, S. S.; Thomas, S. J Appl Polym Sci 1997, 64.
7. Devi, L. U.; Joseph, K.; Manikanada Nair, K. C.; Thomas, S. J Appl Polym Sci 2004, 94, 503.
8. Cantero, G.; Arbelaiz, A.; Mugika, F.; Valea, A.; Mondragon, I. J Reinf Plast Compos 2003, 22, 37.
9. Stamboulis, A.; Ballie, C. A.; Garkhail, S. K.; Van Melick, H. G. H.; Peijs, T. Appl Compos Mater 2000, 7, 273.
10. Rout, J.; Tripathy, S. S.; Mishra, M.; Mohanty, A. K.; Nayak, S. K. Polym Compos 2002, 22, 468.
11. Robson, D.; Hague, J. Presented at the 3rd International Conference on Woodfiber-Plastic Composites, Madison, Wisconsin, 1995.
12. Rowell, R. M.; Han, J. S.; Rowell, J. S. In Natural Polymers and Agrofibres Composites E.L.A.L.A.M. Frolline, L. H. C., Ed. Embrapa Instrumentacao Agropecuaria: Sao Carlos, Brazil, 2000; 115–134.
13. Patel, M.; Bastioili, C.; Marini, L.; Wurdinger, E. Environmental Assessment of Bio-based Polymers and Natural Fibers; Utrecht University: Netherlands, 2002;
14. Mohanty, S.; Verma, S. K.; Tripathy, S. S.; Nayak, S. K. Int Plast Technol 2003, 6, 75.
15. Wong, S.; Shanks, R. A.; Hodzic, H. Macromol Mater Eng 2004, 289, 447.

16. Shah, A. N.; Lakkad, S. C. Fiber Sci Technol 1981, 15, 41.
17. Vaia, R. A.; Ishii, H.; Giannelis, E. P. Chem Mater 1993, 5, 1694.
18. Usuki, A.; Kawasumi, M.; Kojima, Y.; Okada, A.; Kurauchi, T.; Kamigaito, O. J Mater Res 1993, 8, 1174.
19. Usuki, A.; Kojima, Y.; Kawasumi, M.; Okada, A.; Fukushima, Y.; Kurauchi, T.; Kamigaito, O. J Mater Res 1993, 8, 1179.
20. Cho, J. W.; Paul, D. R. Polymer 2001, 42, 1083.
21. Chin, I.; Thurn-Albrecht, T.; Kim, H.; Russell, T. P.; Wang, J. Polymer 2001, 42, 5947.
22. Botev, M.; Betchev, H.; Bikiaris, D.; Panayiotou, C. J Appl Polym Sci 1999, 74, 523.
23. Vaia, R. A.; Price, G.; Ruth, P. N.; Nguyen, H. T.; Lichtenhan, J. Appl Clay Sci 1999, 15, 67.
24. C.C.M. MA. Presented at the First Asian Australasian conference on comporiste materials (ACCM-I), Osaka, Japan, 1998; p 205.
25. Herrera-Franco, P. J.; Valadez-Gonzalez, A. Compos B 2005, 36, 597.
26. Lundin, T.; Cramer, S. M.; Falk, R. H.; Felton, C. J Mater Civil Eng 2004, 16, 547.
27. Ratna, D.; Manoj, N. R.; Varley, R.; Raman, R. K. S.; Simon, G. P. Polym Int 2003, 52, 1403.
28. Bikiaris, D.; Matzinos, P.; Prinos, J.; Flaris, V.; Larena, A.; Panayiotou, C. J Appl Polym Sci 2001, 80, 2877.
29. Foulk, J. A.; Chao, W. Y.; Akin, D. E.; Dodd, R. B.; Layton, P. A. J Polym Environ 2004, 12, 165.
30. Mohanty, S.; Verma, S. K.; Tripathy, S. S.; Nayak, S. K. J Reinf Plast Compos 2004, 23, 625.
31. Rana, A. K.; Mandal, A.; Bandyopadhyay, B. Compos Sci Technol 2003, 31, 143.
32. Lei, Y.; Wu, Q. L.; Clemons, C. M. J Appl Polym Sci 2007, 103, 3056.
33. Ismail, K. In Polypropylene: An A-Z Reference, Karger-Kocsis, J., Ed. Kluwer Academic Publishers: Dordrecht, 1999; 783.
34. Klaus-Peter, M. In Polypropylene: An A-Z Reference, Karger-Kocsis, J., Ed. Kluwer Academic Publishers: Dordrecht, 1999; 527–532.
35. Razdan, S.; Patra, P. K.; Warner, S. Polym Mater Sci Eng 2003, 69, 722.
36. Usuki, A.; Kojima, Y.; Okada, A.; Fukushima, Y.; Kurauchi, T.; Kamigaito, O. J. Mater Res 1993, 8, 1185.
37. Creighton, C. J.; Clyne, T. W. Compos Sci Technol 2000, 60, 525.
38. Yin, S.; Rials, T. G.; Wolcott, M. P. Presented at the Fifth International Conference on Wood Fiber-Plastic Composites, Madison, 1999.;
39. Colom, X.; Carraso, F.; Pages, P.; Canavate, J. Compos Sci Technol 2003, 63, 161.
40. Hashmi, S. A. R.; Kitano, T.; Chand, N. Polym compos 2003, 24, 149.
41. Karger-Kocsis, J. Polypropylene: Structure, Blends and Composites, Vol. 3; Chapman and Hall: London, 1995.
42. Calleja, R. D.; Ribelles, J. L. G.; Padas, M. M.; Greus, A. R.; Colomer, F. R. Polym Compos 1991, 12, 428.